Structured polymer waveguides on distributed Bragg reflector coupling to solid state emitter

2017 J. Opt. 19 065203

(http://iopscience.iop.org/2040-8986/19/6/065203)

OPEN ACCESS
IOP Publishing
Journal of Optics
J. Opt. 19 (2017) 065203 (9pp)
https://doi.org/10.1088/2040-8986/aa6a70

Structured polymer waveguides on distributed Bragg reflector coupling to solid state emitter

Sebastian Knauer[1,2], Martín López-García[2] and John G Rarity[2]

[1] Bristol Centre for Nanoscience and Quantum Information, University of Bristol, Tyndall Avenue, Bristol BS8 1FD, United Kingdom
[2] Department of Electronics and Electrical Engineering, University of Bristol, Merchant Venturers Building, Woodland Road, Bristol, BS8 1UB, United Kingdom

E-mail: John.Rarity@bristol.ac.uk

Received 9 December 2016, revised 10 March 2017
Accepted for publication 31 March 2017
Published 4 May 2017

Abstract

We simulate the coupling of light emitted by a solid state emitter into a structured polymer waveguide. The polymer waveguide is supported on a dielectric mirror making an easy to fabricate platform. This waveguide could be fabricated around a pre-selected and characterized atom like emitter such as a nitrogen vacancy center. We see near deterministic coupling of dipole emitted light into the waveguide and spontaneous emission enhancements up to a factor of 6.2 for TE dipoles coupled to cavity structures.

Keywords: nanophotonics, photonic crystals, coupled resonators, polymer waveguides, microcavity devices

(Some figures may appear in colour only in the online journal)

1. Introduction

Solid state single photon emitters are often non-ideal two level systems with broad spectra due to phonon mediated emission or low quantum efficiencies due to competing non-radiative processes. Coupling the emitter to a photonic structures allows us to modify the spontaneous emission particularly enhancing emission into useful spectral regions [1] and increasing coupling efficiency [2]. Non-ideal solid state emitters could thus be engineered to produce stable on-demand single photons even at room temperature [3] making them useful for quantum information processing [4] and bio-applications [5, 6]. For example single emitters embedded in photonic structures have enabled recent advances in foundational quantum experiments [7–9]. One of the most investigated room temperature solid state emitters is the nitrogen-vacancy (NV) color center. It consists of a substitutional nitrogen atom adjacent to a vacancy in the diamond carbon lattice. This system exists stably in the singly charged state and possesses a ground state spin which can be initialized and read out optically. Stable NV emission with long spin coherence times has been reported in bulk [10] and in nanometer scale diamond particles (nanodiamonds) [11]. These latter NV centers can be incorporated in, and thus coupled to photonic structures [12]. One fast and cost effective method for the fabrication of such photonic structures, especially cavities, is direct laser writing in photopolymers. They have been reported as nanobeam cavities [13, 14] or droplet whispering gallery modes [15]; coupling of NV centers to whispering gallery modes of resonator disks are reported in [16]. These polymer structures are designed for room temperature applications, but may also be used at cryogenic temperatures [17]. However, these methods incorporate nanodiamonds suspended in the polymer and lead to non-deterministic positioning of the emitters in the photonic structure and use air guiding to achieve strong confinement. Hence structures are suspended in air with associated fabrication difficulties and a lack of robustness.

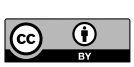

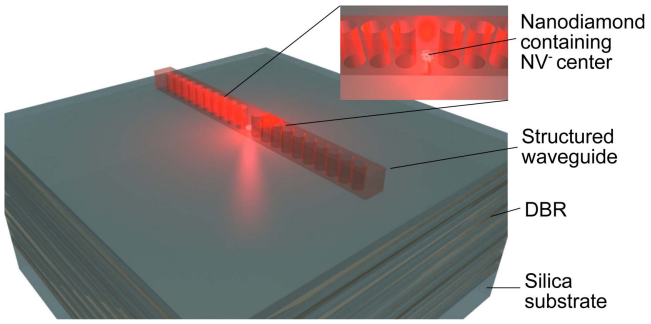

Figure 1. Concept: the image shows the proposed device including distributed Bragg reflector, substrate and structured waveguide for the coupling to a single photon emitter.

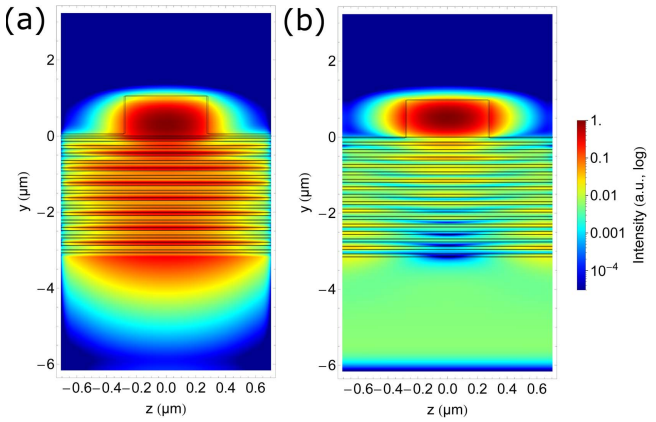

Figure 2. Intensity ($|E|^2$) profile of a polymer waveguide ($n = 1.52$) on top of the SiO_2/ Ta_2O_5 DBR (fundamental modes) and silica substrate as indicated in figure 1. (a) Mode01 is characterized by an effective refractive index of $n_{\mathrm{eff,wg}} = 1.437$ and an in-plane polarization fraction of $E_y \approx 100\%$ (quasi TM waveguide mode). Allowing losses into the silica substrate leads to a value of about 0.007 dB cm^{-1}. (b) Mode02 is characterized by an effective refractive index of $n_{\mathrm{eff,wg}} = 1.412$ and a in-plane polarization fraction of $E_y \approx 0\%$ (quasi TE waveguide mode). Allowing losses into the silica substrate leads to a value of about 366 dB cm^{-1}. Note the logarithmic color coded intensity used to highlight that the TE mode extends all the way through the substrate, leading to high losses.

In this work we use the Bragg confinement of a supporting mirror to confine the light in surface waveguides designed to be written in polymer using direct write methods. We present modeling results for the coupling of NV centers in nanodiamonds to microstructured waveguide cavities as illustrated in figure 1. The NV centers are placed near the surface of the substrate, allowing optical characterization and localization followed by direct writing of microstructured waveguides over them. We suppress the losses into the substrate by using a suitably designed distributed Bragg reflector. These structures may then allow top-coupling via commonly used integrated grating couplers or standard waveguide edge couplers. Further, this design benefits from its small dimensions allowing, for bio-applications, the use of small analyte volumes and coupling to microfluidic channels [18].

2. Design of passive structured waveguide

We optimize the structure by the following steps:

1. Design the DBR.
2. Optimize the nanobeam polymer waveguide.
3. Design simple reflectors in the waveguide.
4. Modeling a tapered reflector.

The design of the DBR has been guided by the premise of a wide stop band reaching from 600 to 750 nm with a center wavelength of 660 nm. This bandgap is designed to maintain high reflectivity at 637 nm out to high incidence angles. Silicon dioxide (SiO_2) with a refractive index of $n_{SiO_2} = 1.54$ is used as low index quarter wavelength top layer to ensure an antinode at the mirror surface. This is then alternated with tantalum pentoxide (Ta_2O_5) with a refractive index of $n_{Ta_2O_5} = 2.03$ with a total sixteen pairs to ensure over 99.9% reflectance (mid band normal incidence).

Using a commercial-grade simulator eigenmode solver and propagator (Lumerical Solutions) the polymer waveguide structure ($n = 1.52$) has been optimized with the aim to maintain a waveguided mode highly confined within the polymer [19, 20]. Note that the small refractive index contrast of suitable materials in the visible spectral range might reflect on a less confined mode than in similar designs for the NIR range [19]. Iterating width w in the range of 420–620 nm and height h in the range of 400–1400 nm of the waveguide, optimal parameters are found with $w = 0.56$ μm and a height of $h = 1$ μm at 637 nm (zero-phonon line NV^- center). Here, the peak amplitude of the electrical field associated with the guided mode is confined within the polymer is maximized. These conditions are necessary to obtain a strong light–matter interaction at the position of the solid state emitter, i.e. interface of NV^- center and propagating mode. For a well confined single mode on the DBR surface we chose a rectangular cross section, allowing smallest fabrication dimensions with laser polymer lithography. In the following the two waveguide modes which show the highest confinement within the waveguide are discussed figure 2.

Both modes can be distinguished by their effective waveguide refractive indices $n_{\mathrm{eff,wg}}$, their in-plane polarization fraction E_y as well as their losses into the silica substrate where relevant. The two-dimensional in-plane polarization fraction E_y, is defined over

$$\frac{\int |E_y|^2 \mathrm{d}z\mathrm{d}y\mathrm{d}x}{\int (|E_y|^2 + |E_z|^2)\mathrm{d}z\mathrm{d}y\mathrm{d}x}, \tag{1}$$

where $E_{y,z}$ refer to the field components in y direction (z direction respectively). Since we are considering the polarization of the modes, we only consider the fields parallel to the mode cross section and components in E_x are neglected. As shown in figure 3 the dispersion relations for both modes

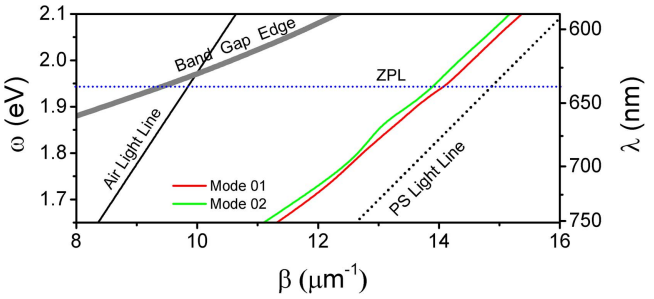

Figure 3. Dispersion curves for mode01 (quasi-TM, red line) and mode02 (quasi-TE, green line) in figure 2 with β the wavenumber. Thin solid and dotted lines show light lines for air and bulk polymer respectively. The thick gray line shows the photonic bandgap edge for the DBRs considered in this study. Reflectance of the DBR is close to 1 for energies higher than the band gap edge. The zero-phonon line (ZPL) indicates the energy ($\omega = 1.64$ eV, $\lambda = 637$ nm) for which the modes described in this work have been optimized.

lie within the light cones of air and bulk polymer denoting total confinement within the structure for the ZPL. Both modes are very similar to those obtained from a polymer free standing waveguide, but with a smaller effective refractive index. The modes lie below the mirror band edge indicating that although highly reflective at normal incidence there will be some leakage at the low incidence angles of guided modes. Mode01 is characterized by $n_{\mathrm{eff,wg}} = 1.437$ and $E_y \approx 100\%$ (quasi TM waveguide mode) and mode02 by $n_{\mathrm{eff,wg}} = 1.412$ and $E_y \approx 0\%$ (quasi TE waveguide mode). Therefore care has to be taken in choosing the appropriate mode for the coupling to the later discussed TE (E_z orientated) and TM dipole (E_y orientated). Allowing the mode to be unbounded in the direction of the silica substrate, i.e. allowing absorption in a perfect matched layer, one obtains losses for mode01 of 0.007 dB cm^{-1} and for mode02 366 dB cm^{-1}. This dramatic difference in loss characteristics can be seen in the logarithmic intensity profiles. The quasi TE mode (figure 2) is concentrated in the waveguide but extends at an approximate 0.3% level all the way to the lower boundary in the silica substrate indicating significant losses. On the other hand the quasi TM mode exists as a mode guided by the ridge and DBR combined and does not extend into the substrate. Despite this when we consider waveguide lengths of 40–50 μm both modes show low enough loss. Other modes are also supported by the waveguide-DBR combined structure but these were not well confined in the waveguide and therefore not useful for the coupling to single emitters at the interface between the polymer waveguide and DBR.

To achieve a strong interaction of the dipole emitter with the waveguide mode we place reflectors in the waveguide arranged to created a resonant cavity. We choose to study circular reflectors as these are easier to fabricate using direct write methods and have shown high reflectivity in suspended cavity designs [21]. Firstly, the transmission of reflectors in the structured waveguide is calculated. This includes the optimization of the filling fraction f and the reflector period in the x-direction a_x. The right hand half of the structure shown in figure 4, is studied. For this optimization thirty circular reflector holes have been placed in the waveguide. The spatial

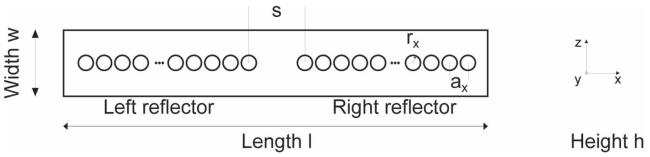

Figure 4. Waveguide structure with reflectors. The modes in the waveguide have been optimized for a width $w = 0.56$ μm and a height of $h = 1$ μm. The values r_x, a_x and s indicate the reflector radius, the reflector spacing and the cavity distance.

mode profile at the center wavelength is calculated with the eigenmode solver and then injected at all wavelengths, leading to a very small injection error around the center wavelength. The transmission of the quasi TM and TE waveguides modes have been measured over the entire structure by FDTD methods. The number of reflectors are chosen in order to ensure a high reflectivity but still having low losses. The results have been normalized by the transmission of the modes through the empty waveguide over the same distance. A central wavelength λ_c at 637 nm (zero-phonon line NV center)[3] is chosen to calculate the appropriate reflector distance with

$$a_x = \frac{\lambda_c}{2n_{\mathrm{eff}}}. \tag{2}$$

This distance relates to the hole radius over

$$r_x = \sqrt{\frac{1}{\pi} a_x w f}. \tag{3}$$

For the calculation of the appropriate reflector radius an effective refractive index n_{eff} is approximated using

$$n_{\mathrm{eff}} = \sqrt{f n_{\mathrm{eff,r}}^2 + ((1-f) n_{\mathrm{eff,wg}}^2)}, \tag{4}$$

where the effective reflector refractive index is approximated $n_{\mathrm{eff,r}} = 1$ and f is the filling fraction of the unit cell covered by the reflector holes. The filling fraction is varied between 0 and 0.3 and the transmission in the wavelength range 597–677 nm is measured behind the reflectors. For a filling fraction greater than 0.3 the reflector holes start to merge with each other. The results are shown in figures 5(a)–(c) (mode01) and figures 5(d)–(f) (mode02). Mode01 shows a strong transmission suppression over a wavelength range of about 610–650 nm (figure 5(e)). Further, this mode exhibits a constant transmission suppression over a wide filling fraction range. Due to the higher guidance of the mode in the DBR pairs the influence of the reflectors for the propagating mode is reduced. The transmission is about 30% at a the central wavelength figures 5(a)–(c). A filling fraction of 0.13 (radius of 75 nm) is chosen to model the radius of the waveguide reflectors.

The modulation of the filling fraction for mode02 shows a stop band opening from 605 to 670 nm which is wider than the one for mode01 figures 5(d)–(f). An optimal value for the transmission suppression down to $\leqslant 0.1\%$ can be achieved at a

[3] Note: Maxwell's equation are scale invariant. Hence applying a scaling factor allows the results to be changed to any wavelength (e.g. phonon side bands of the NV center).

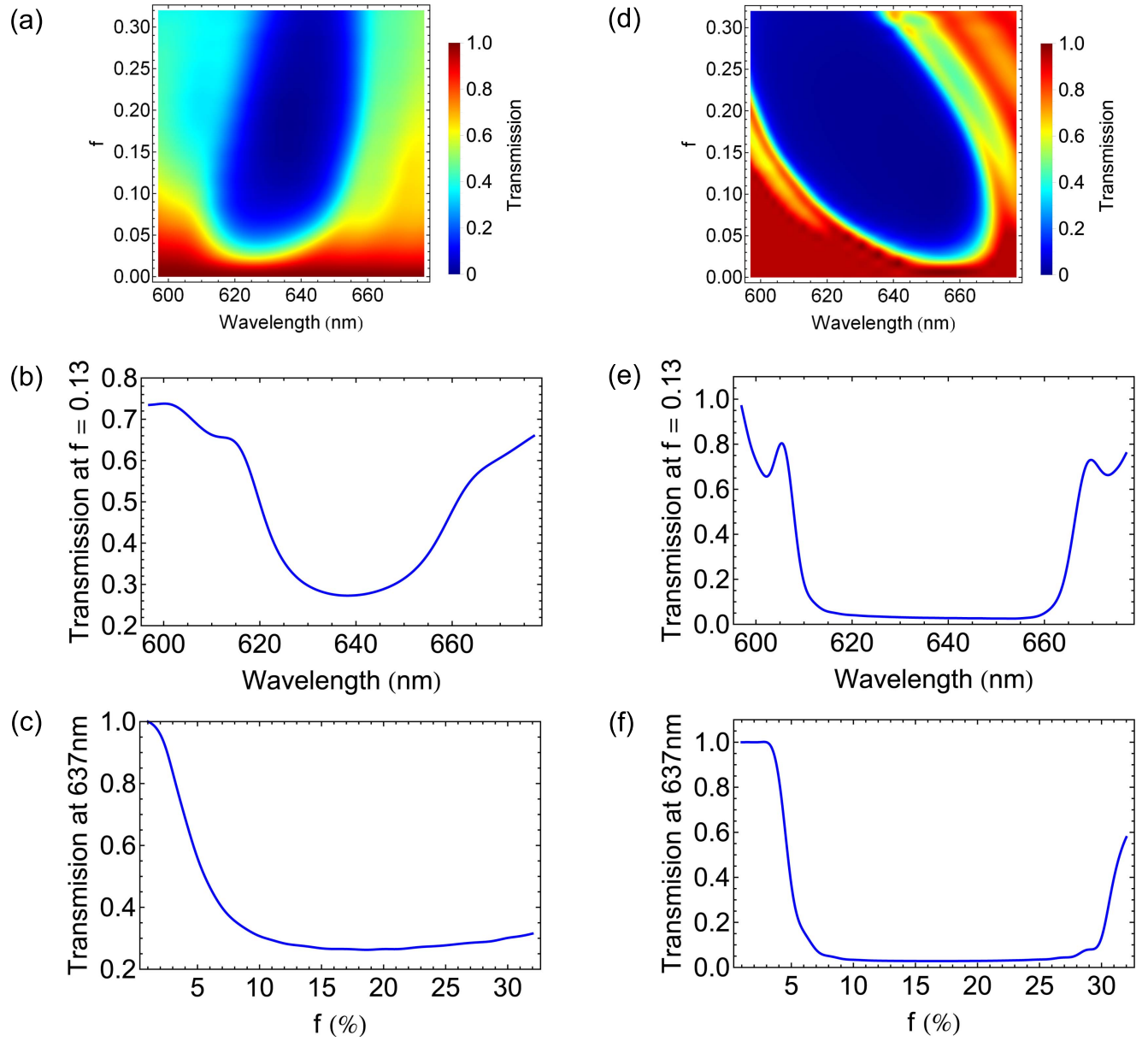

Figure 5. Transmission through the waveguide varied over wavelength and filling fraction f ((a) mode01, (d) mode02). Transmission at a filling fraction of 0.13 for different wavelengths ((b) mode01, (e) mode02). Transmission at a wavelength of 637 nm for different filling fractions ((c) mode01, (f) mode02). The data is normalized to the transmission through the empty waveguide. Mode01 is characterized by a narrow stop band and a minimum transmission of 30%, while mode02 possesses a wide stop band ranging from 615 to 665 nm and a minimum transmission of $\leqslant$0.1%.

filling fraction of 0.13. Further, the transmission is suppressed over a wider filling fraction range compared to mode01 (figure 5(c)) due to the field profile being primarily confined within the polymer waveguide.

Losses in the waveguide reflectors are studied as a function of number of holes. These losses are illustrated by measuring the cavity transmission on resonance, shown in figure 6(a) for mode02. The quasi waveguide modes are launched into the structure and the transmission is measured behind the reflector holes over the entire structure with optimized cavity distance. The results show that an upper bound for number of reflector holes can be set where the mode losses dominate. The cavity resonance peak initially narrows with increasing hole numbers but reaches a saturation and remains a constant width but with reducing overall transmission as the hole losses dominate (figure 6(b)). In comparison an equivalent simulation for mode01 is not possible, because a significant fraction of the mode propagates in the distributed Bragg reflector below the structure. Mode01 is limited by the mirror strength (figure 5(b)) and a cavity peak is not visible in the stopband over the left and right reflector side. Therefore mode02, although having initially more substrate losses (figure 2(b)), seems to be more feasible for guidance in longer waveguide structures. However, we will discuss in the next section figure 7 that for both modes an emitting dipole at the cavity center excites a well defined local cavity mode.

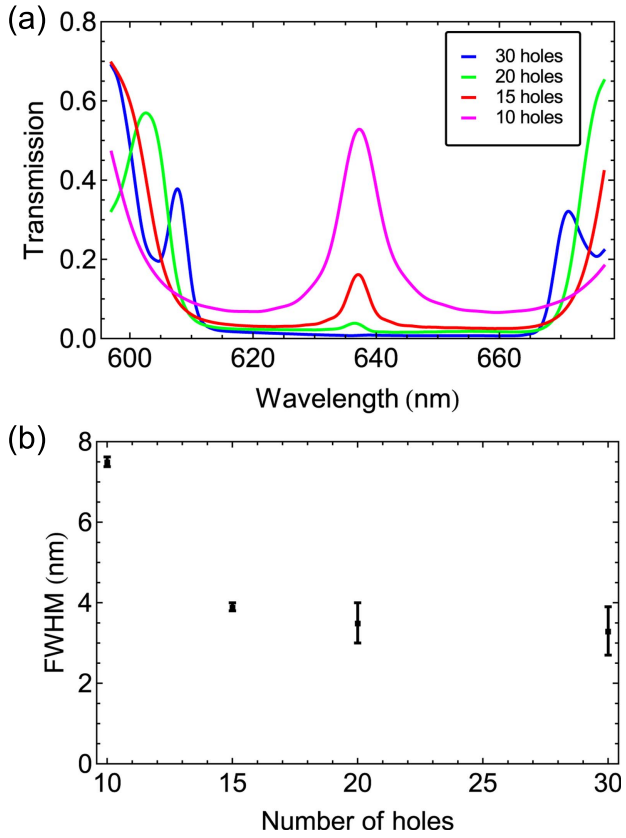

Figure 6. (a) Transmission through the symmetric structured waveguide and cavities with the optimized parameter of a cavity distance 582 nm and a filling fraction of 0.13. The number of reflector holes has been varied. (b) FWHM of the cavity peak in (a) obtained with a Lorentz fit.

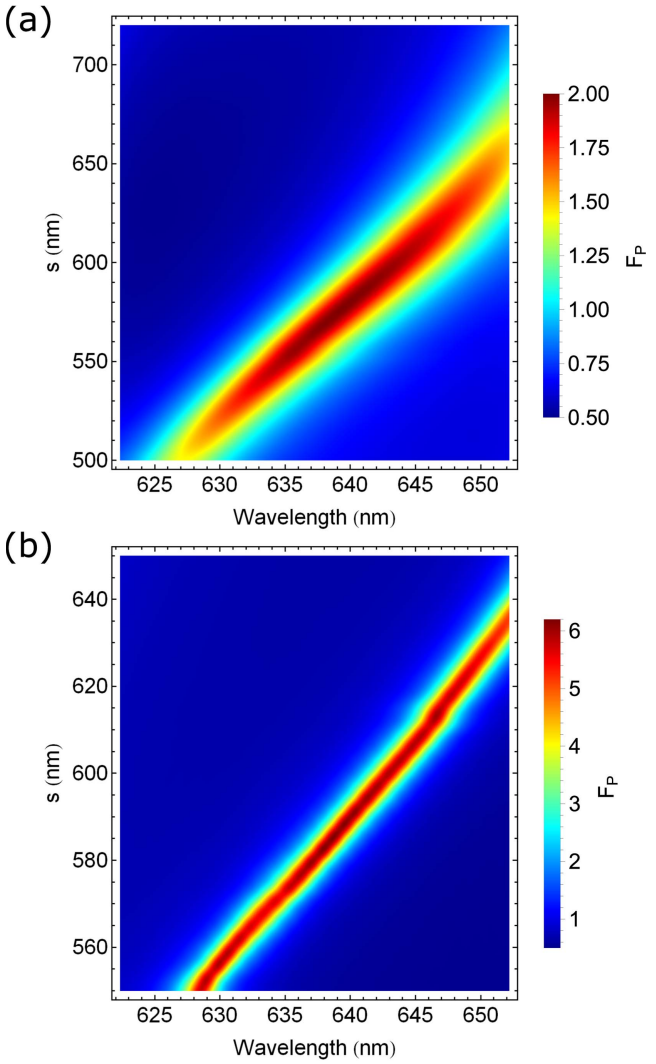

Figure 7. Purcell factor over the variation of the cavity distance s and wavelength for the 50 hole symmetric structured waveguide: (a) mode01 excited with TM dipole, (b) mode02 excited with TE dipole. The structure is excited with a dipole with a pulse length of 20 fs at 637 nm. This leads to an optimal cavity distance of $s = 562$ nm and a Purcell factor of 2.2 for the TM ($s = 582$ nm and a Purcell factor of 6.1 for the TE dipole respectively).

3. Coupling to single emitter

The two cases of a TE (field polarization direction parallel to surface) and a TM (field polarization direction perpendicular to surface) dipole, emulating the extreme cases of the single solid state emitter orientation, are investigated. The dipoles with a center frequency of 470.6 THz (637 nm) and a pulse length of 20 fs have been placed at the position of the maximum field intensity to ensure the stronger cavity mode-dipole interaction. In the following simulations we assume an ideal dipole not perturbed by a nanocrystal containing the dipole itself. However, for the later discussed case in figures 7(a) and (b) we additionally place a 20 nm disdyakis dodecahedron nanocrystal (refractive index 2.4) around the dipole and find out that the results differ by less than one percent compared to the ideal dipole.

The dipole emission rate is proportional to the local density of states which can lead to emission enhancement (or suppression), depending on the dipole position within the structure as first proposed by Purcell for radio waves [22] and later adopted by the optics community analyzing changes in spontaneous emission [23, 24]. The Purcell factor is a measure of this enhancement with respect to unstructured environments and thus is a good figure of merit to compare structures. Here we calculate it by the standard method [25] of taking the ratio of total power emitted (at a particular wavelength) to total power emitted when the emitter is embedded in homogeneous polymer. We show false color plots of the Purcell factor as a function of cavity length and wavelength in figure 7(a) (waveguide mode01 with TM dipole) and figure 7(b) (waveguide mode02 with TE dipole). The Purcell factor has been calculated directly over the emitted dipole power normalized by the power emitted in a homogeneous polymer environment. In the optimization the peak Purcell factor is taken at the cavity resonance. The TM dipole excited cavity mode01 exhibits a Purcell factor up to 2.2. The optimal cavity distance is hereby 562 nm at a center wavelength of 637 nm. The TE dipole excite mode02 reaches a Purcell factor of up to 6.1 at an optimal cavity distance of 582 nm.

To investigate the coupling of the TM dipole (waveguide mode01) and the TE dipole (waveguide mode02) to the structured waveguide, we measure the Purcell factor and the

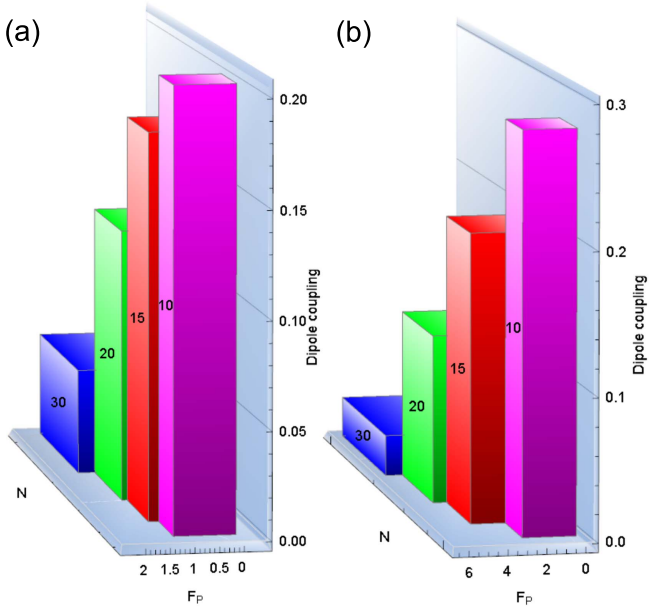

Figure 8. Purcell factor and normalized dipole coupling in dependence of the reflector hole number N ((a) structured waveguide mode01 with TM dipole, (b) structured waveguide mode02 with TE dipole).

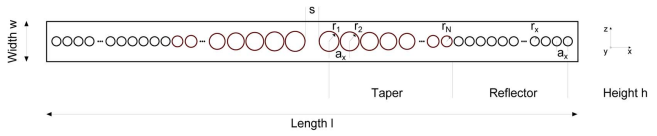

Figure 9. Waveguide structure with reflectors. The structure consists of a tapered and a reflector region. For more details see text.

dipole coupling as a function of the number of reflectors N in figure 8. The coupling efficiency into mode01 and modes02 is calculated as the ratio between total power coupled into each of those modes after dipole excitation of the cavity with the total power emitted by the dipole. The power emitted into waveguide modes is measured one lattice constant behind the last hole on a single reflector side. We find coupling efficiencies of 0.2 for the TM dipole (waveguide mode01) and of 0.28 for the TE dipole (waveguide mode02) in the case of a 10 hole reflector, which leads to a total cavity mode efficiency of 40% and 56%. However, these efficiencies decrease rapidly with increasing number of holes and Purcell factor.

In the following the structured waveguide will be further optimized. We keep the 30 hole reflector as studied above and add a hole taper close to the cavity. The waveguide coupled mode02 TE dipole has a higher coupling efficiency to the cavity. It is therefore selected for the optimization. In the following we study the effect of a quadratic taper [13] with decreasing reflector size figure 9. Other forms of tapering (e.g. [26]) are less suitable for the material system and hence the low effective refractive index in the work presented here. The reflector radius of 75 nm shown above is feasible with current fabrication techniques. However, further radius reduction remains challenging. To minimize the scattering losses a 4–15 hole taper is studied. The reflector hole spacing a_x is kept constant in the taper section while the cavity spacing s is

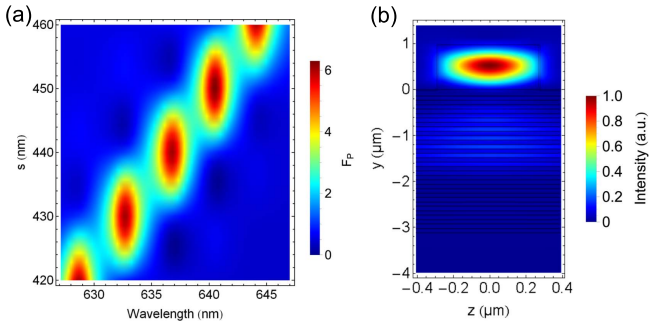

Figure 10. (a) Purcell factor modeled over the wavelength with nine tapered holes for mode02. The maximum filling fraction for the biggest reflector is found with 0.18. A Purcell factor of 6.1 is achieved. (b) Intensity ($|E|^2$) profile of the TE dipole excited mode02 in the transition between taper and reflector.

varied between 420 and 460 nm to accommodate the change in the filling fraction of the closest reflector to the cavity. This end filling fraction associated with the hole radius r_1 in figure 9 is swept from 0.18 to 0.25 in single steps aiming for a high reflector strength. This range is chosen from the stop band shown in figure 5(f).

A high reflection is maintained within the stop band without a merging of the holes due to the increased diameter, to identify the maximum Purcell factor at the desired resonance wavelength of 637 nm. For a robust design we have extended the length of the taper to its maximum values in which the Q-factor saturates. Thus the Q-factor is limited by the scattering losses and should not be strongly influenced by fabrication tolerances. The Purcell factor at the resonance frequency 637 nm increases up to 6.2 which is higher than for the untapered case. The optimal taper for waveguide coupled mode02 TE dipole a taper with 9 reflector holes can be modeled while still maintaining a high Purcell factor of 6.1 at the design frequency of 637 nm. The optimal filling fraction is hereby 0.18, which leads to a hole radius of $r_1 = 88$ nm. An example for the optimization is found in figure 10(a) (the discrete steps originate from the sweep resolution). The structure at the resonance with the highest Purcell factor is given at a cavity length of 440 nm. During the optimization process we have ensured that the mode is well confined within the waveguide. An example for the mode intensity profile ($|E|^2$) in the transition region between taper and reflector is given in figure 10(b). Given that mode02 (TE dipole coupling) exhibits a higher Purcell factor we show in figure 11 the spectrum and field decay of the full tapered cavity structure excited with discussed optimal parameters. The plots confirm that the structures are single mode at 637 nm. The structures have quality factors of $Q = 220$ for mode02 calculated over the field decay of the time signal figure 11(b). Thus, the taper provides an improvement compared to the non-tapered cavity, which led to $Q = 190$ (data not shown). Mode02 intensity plots on cavity resonance are shown in figure 12. The measured intensities allow us to calculate the mode volume of the optimized structures with $V = 0.195\ \mu\text{m}^3$ for mode02 ($V = 0.21\ \mu\text{m}^3$ for mode01). We can combine mode volumes and quality factors to calculate a

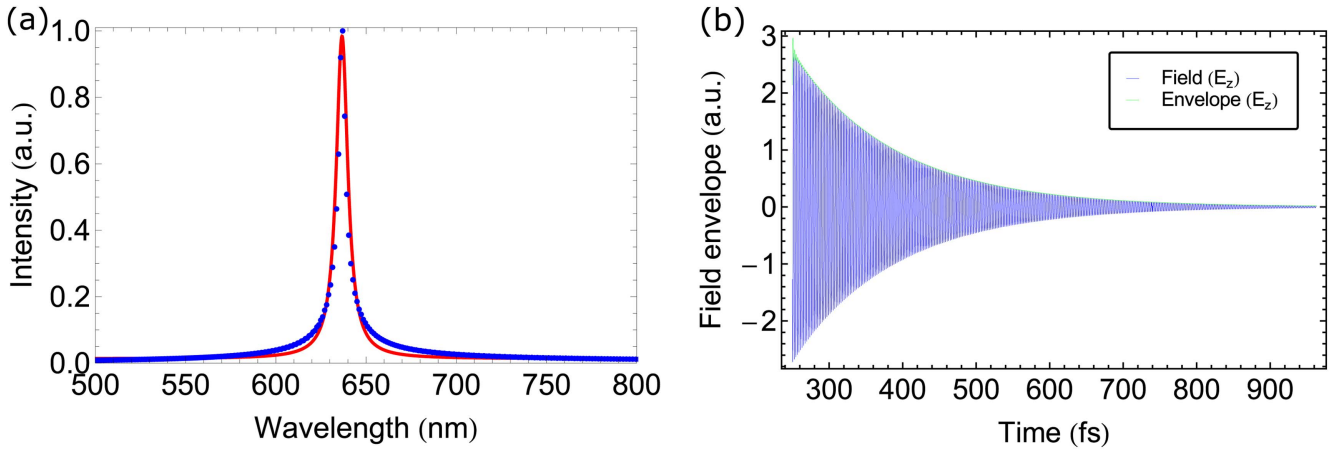

Figure 11. Spectrum of mode02 (TE dipole coupling) with nine tapered holes, end filling fraction of 0.18 and a cavity distance of 440 nm. A Lorentzian fit is used.

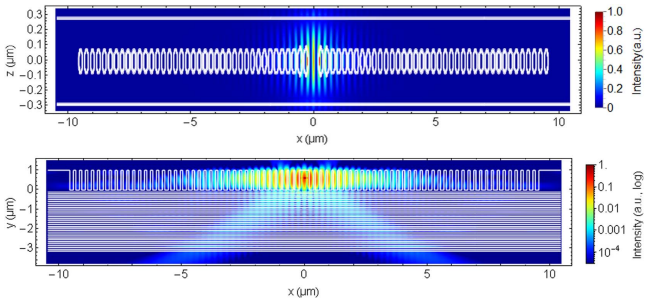

Figure 12. Intensity profile across the structured waveguide in the x/z-plane (top) and x/y-plane (log, bottom) for mode02. Compared to mode01 (not shown) this mode has lower losses into the z-direction. Only a small percentage enters the distributed Bragg reflector.

predicted Purcell factor using [27]

$$F_{\mathrm{P}} = \frac{3}{4\pi^2}\left(\frac{\lambda_{\mathrm{r}}}{n_{\mathrm{eff}}}\right)^3 \frac{Q}{V}, \tag{5}$$

where λ_{r} represents the resonance wavelength and n_{eff} the effective refractive index. This result independently confirms our Purcell factor estimates of 6.1. With these Purcell factors a shorter excited state lifetime can be achieved, leading to an enhanced emission rate up to 20% at the zero-phonon line of the NV^- center for the perfect coupled TE dipole (mode02). As pointed out, the design is scalable to other wavelengths, e.g. the phonon side bands of the NV^- center.

In figure 12(a) we observe that the interaction of the emitted light of the dipole with the DBR substrate is minimal (not shown for mode01). The interaction and the losses of mode02 on the DBR substrate are lower than for mode01. The source of the main losses for both modes are due to the low refractive index contrast and thus transmission and scattering losses. Although the increase in Purcell factor is small, one advantage of the tapered holes is the bigger hole radius near the dipole, making fabrication more reproducible. Note that the structure presented here supports several modes confined within the DBR rather than the polymer waveguide. Thus, the dipolar excitation of the cavity can lead to the excitation of other modes besides the fundamental ones

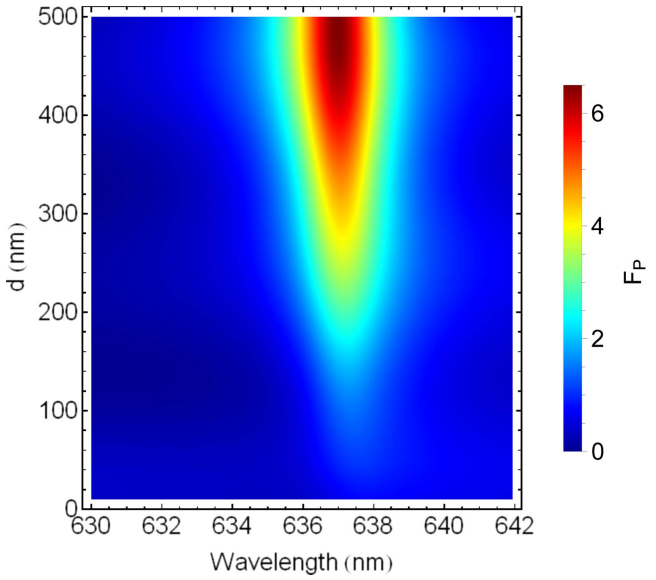

Figure 13. Sweep of the TE-dipole position d from the DBR surface within the optimized structured waveguide. The Purcell factor is recorded.

described in section 2. However, the high Purcell factors (figure 7) and the field profiles after cavity excitation with a dipole (figure 12) show that coupling into non-fundamental modes is negligible for the optimized structure.

Finally, we investigate the dipole position d from the DBR surface within the optimized structured waveguide and record the Purcell factor figure 13. The dipole position analyzed between 10 and 500 nm. We observe at the resonance wavelength of 637 nm for both modes that the Purcell factor drops from its optimal value down to values around 1.2. Therefore we propose two experimental methods. Either nanodiamond with a size around 30–120 nm are used and one obtains moderate Purcell factors between 1.5 and 2. These nanodiamond sizes have been shown to contain single NV centers. In the alternative approach one uses a semi-deterministic method. We propose to include the nanodiamonds within the photoresit, as performed in [16], and writing multiple waveguides. Before writing the cavity in a second fabrication process,

nanodiamonds containing single NV^- centers in the waveguides are optically addressed and characterized. Here, the probability is higher that the nanodiamonds are centers within the waveguide and would lead to the higher Purcell factors.

In future designs we would aim to utilize a Bragg reflector such that the ZPL fully falls between the air-light line and the mirror edge, allowing us to explore lower loss modes (e.g. Bloch) to achieve higher Purcell factors [19].

4. Conclusion

Engineering strongly guiding photonic structures usually requires the development of suspended geometries and deterministic incorporation of single emitters at cavity center is a challenge. Here we use the Bragg confinement of a supporting mirror to confine the light in surface waveguides designed to be written in polymer using direct write methods. We have demonstrated two designs for cavities in such waveguides and optimized their utility for single emitter coupling by maximizing Purcell factors at the cavity center on resonance, achieving a maximum Purcell factor of 6.2. The large cavity spacing (between mirrors) make deterministic incorporation of an emitter straightforward. For instance, initially one might place (e.g. spin-coat) many emitters slightly above the mirror substrate, characterize and localize suitable emitters and then write the cavity waveguides around them. In the experimental realization a high control in the dipole positioning may allow the scaling of the waveguide and thus lower losses through the polymer surface.

The smallest feature size presented in this paper is a radius of 75 nm (diameter of 150 nm), which is achievable with current commercially available two-photon absorption lithography [28]. Hence we expect fabrication of our structures to be reasonably straightforward. However, novel techniques are extending two-photon lithography to resolution far below 100 nm [29, 30]. We also note that the interaction of the lithography laser and the DBR substrate, will alter the required incident power most probably reducing it.

In our simulations two cases of a TE and a TM orientated dipoles were investigated. With our designs we allow the flexibility in the fabrication of the reflectors in the structured waveguide while maintaining the Purcell factor. Our optimized structures will have applications in the development of spin photon interfaces for quantum information processing [31] and bio-sensing (magnetic and optical) using microfluidics.

Acknowledgments

This work has been funded by the project 'WASPS', which acknowledges the financial support within the Seventh Framework Programme for Research of the European Commission, under FET-Open grant number: FP7-618078. JGR is sponsored under EPSRC grant No.EP/M024458/1.

References

[1] Riedrich-Möller J *et al* 2012 One- and two-dimensional photonic crystal microcavities in single crystal diamond *Nat. Nanotechnol.* **7** 69–74
[2] Hadden J P, Harrison J P, Stanley-Clarke A C, Marseglia L, Ho Y L D, Patton B R, O'Brien J L and Rarity J G 2010 Strongly enhanced photon collection from diamond defect centres under micro-fabricated integrated solid immersion lenses *Appl. Phys. Lett.* **97** 1–3
[3] Kurtsiefer C, Mayer S, Zarda P and Weinfurter H 2000 Stable solid-state source of single photons *Phys. Rev. Lett.* **85** 290–3
[4] Bukach A A and Kilin S Y 2010 Creation of entangled state between two spaced NV centers in diamond *Opt. Spectrosc.* **108** 254–66
[5] Hall L T *et al* 2012 High spatial and temporal resolution wide-field imaging of neuron activity using quantum NV-diamond *Sci. Rep.* **2** 1–9
[6] Balasubramanian G, Lazariev A, Arumugam S and Duan D W 2014 Nitrogen-vacancy color center in diamond-emerging nanoscale applications in bioimaging and biosensing *Curr. Opin. Chem. Biol.* **20** 69–77
[7] Bernien H, Childress L, Robledo L, Markham M, Twitchen D and Hanson R 2012 Two-photon quantum interference from separate nitrogen vacancy centers in diamond *Phys. Rev. Lett.* **108** 1–7
[8] Sipahigil A, Goldman M, Togan E, Chu Y, Markham M, Twitchen D, Zibrov A, Kubanek A and Lukin M 2012 Quantum interference of single photons from remote nitrogen-vacancy centers in diamond *Phys. Rev. Lett.* **108** 1–5
[9] Hensen B *et al* 2015 Loophole-free Bell inequality violation using electron spins separated by 1.3 kilometres *Nature* **625** 682–6
[10] Gaebel T *et al* 2006 Room-temperature coherent coupling of single spins in diamond *Nat. Phys.* **2** 408–13
[11] Knowles H S, Kara D M and Atatüre M 2014 Observing bulk diamond spin coherence in high-purity nanodiamonds *Nat. Mater.* **13** 21–5
[12] Barth M, Schietinger S, Schröder T, Aichele T and Benson O 2010 Controlled coupling of NV defect centers to plasmonic and photonic nanostructures *J. Lumin.* **130** 1628–34
[13] Quan Q, Burgess I B, Tang S K Y, Floyd D L and Lončar M 2011 Deterministic design of wavelength scale, ultra-high Q photonic crystal nanobeam cavities *Opt. Express* **19** 258–65
[14] Tadayon M A, Baylor M E and Ashkenazi S 2014 High quality factor polymeric Fabry–Perot resonators utilizing a polymer waveguide *Opt. Express* **22** 5904–12
[15] Ta V D, Chen R and Sun H D 2013 Tuning whispering gallery mode lasing from self-assembled polymer droplets. *Sci. Rep.* **3** 1362
[16] Schell A W, Kaschke J, Fischer J, Henze R, Wolters J, Wegener M and Benson O 2013 Three-dimensional quantum photonic elements based on single nitrogen vacancy-centres in laser-written microstructures *Sci. Rep.* **3** 1–19
[17] Lee C, Choi H, Gu E, Dawson M and Murphy H 2006 Fabrication and characterization of diamond micro-optics *Diam. Relat. Mater.* **15** 725–8
[18] Estevez M C, Alvarez M and Lechuga L M 2012 Integrated optical devices for lab-on-a-chip biosensing applications *Laser Photon. Rev.* **6** 463–87
[19] Liscidini M 2012 Surface guided modes in photonic crystal ridges: the good, the bad, and the ugly *J. Opt. Soc. Am.* B **29** 2103–9
[20] Lumerical Solutions, Inc. http://lumerical.com/tcad-products/mode/ (accessed: 2013–2016)
[21] Zhang Y, McCutcheon M W, Burgess I B and Lončar M 2009 Ultra-high-Q TE/TM dual-polarized photonic crystal nanocavities *Opt. Lett.* **34** 2694

[22] Purcell E M 1946 Spontaneous emission probabilities at radio frequencies *Phys. Rev.* **69** 246–60
[23] Yablonovitch E 1987 Inhibited spontaneous emission in solid-state physics and electronics *Phys. Rev. Lett.* **58** 2059–62
[24] Lodahl P, Floris Van Driel A, Nikolaev I S, Irman A, Overgaag K, Vanmaekelbergh D and Vos W L 2004 Controlling the dynamics of spontaneous emission from quantum dots by photonic crystals *Nature* **430** 654–7
[25] Ho Y L D, Cao T, Ivanov P S, Cryan M J, Craddock I J, Railton C J and Rarity J G 2007 Three-dimensional FDTD simulation of micro-pillar microcavity geometries suitable for efficient single-photon sources *IEEE J. Quantum Electron.* **43** 462–72
[26] Velha P, Picard E, Charvolin T, Hadji E, Rodier J C, Lalanne P and Peyrade D 2007 Ultra-high Q/V Fabry–Perot microcavity on SOI substrate *Opt. Express* **15** 16090–6
[27] Englund D, Fattal D, Waks E, Solomon G, Zhang B, Nakaoka T, Arakawa Y, Yamamoto Y and Vučković J 2005 Controlling the spontaneous emission rate of single quantum dots in a two-dimensional photonic crystal *Phys. Rev. Lett.* **95** 013904
[28] Nanoscribe, Inc. http://nanoscribe.de/en/
[29] Gan Z, Cao Y, Evans R A and Gu M 2013 Three-dimensional deep sub-diffraction optical beam lithography with 9 nm feature size *Nat. Commun.* **4** 1–7
[30] Wollhofen R, Katzmann J, Hrelescu C, Jacak J and Klar T A 2013 120 nm resolution and 55 nm structure size in STED-lithography *Opt. Express* **21** 10831–40
[31] Young A, Hu C Y, Marseglia L, Harrison J P, O'Brien J L and Rarity J G 2009 Cavity enhanced spin measurement of the ground state spin of an NV center in diamond *New J. Phys.* **11** 013007